Supplemental Information for:

Hydrogen Peroxide Disproportionation with Manganese Macrocyclic Complexes of Cyclen and Pyclen

David M. Freire,[a] Debora Beeri,[a] Kristof Pota,[a] Hannah Johnston,[a] Philip Palacios,[b] Brad S. Pierce,[c] Benjamin Sherman,[a] Kayla N. Green [a,*]

[a] Department of Chemistry and Biochemistry, Texas Christian University, 2950 W. Bowie, Fort Worth, TX 76129, United States

[b] Department of Chemistry and Biochemistry, The University of Texas at Arlington, 700 Planetarium Place, Arlington, TX 76019

[c] Department of Chemistry and Biochemistry, University of Alabama, 250 Hackberry Lane, Box 870336 Tuscaloosa, AL 35487

Table of Contents

Table S1. Protonation constants[a] of cyclen and pyclen (I = 0.15 M NaCl and T = 298 K).

	cyclen	**pyclen**[b]
log K_1^H	10.81(1)	11.37
log K_2^H	9.66(2)	8.22
log K_3^H	0.88(2)	1.61
∑ log K_i^H	21.35	21.20

[a]Defined as $K_i^H = [H_iL^{i+}]/([H^+][H_{i-1}L^{(i-1)+}])$ for i = 1-3, [b] ref. [1]

Table S2. Overall stability constants (log β_{pqr}) of Mn(II) complexes (I = 0.15 M NaCl and T = 298 K). Charges are omitted for clarity.

Equilibrium quotient	**cyclen**	**pyclen**
[MnL]/([Mn][L])	8.34(2)	10.11(4)
[ML]/([M(OH)L][H])	10.22(6)	11.01(5)

Table S3. Crystal data, Intensity Collections, and Structure Refinement Parameters for $[Mn(pyclen)Cl_2][ClO_4]$ and $[Mn_2(pyclen)_2(\mu\text{-}O)_2][ClO_4]_3$.

Complex	$[Mn(pyclen)Cl_2][ClO_4]$ 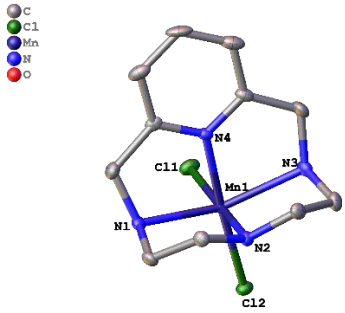	$[Mn_2(pyclen)_2(\mu\text{-}O)_2][ClO_4]_3$ 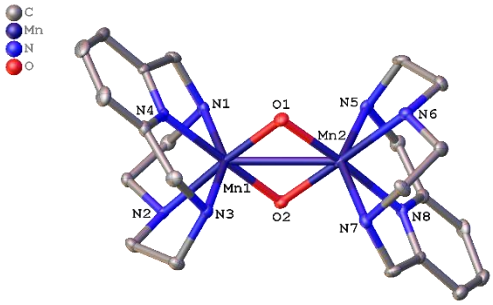
Empirical formula /Asymmetric Unit	$C_{11}H_{18}Cl_3MnN_4O_4$	$C_{22}H_{44}Cl_3Mn_2N_8O_{18}$
Formula weight	431.58	924.88
Temperature/K	100.(2)	100.(2)
Crystal system	monoclinic	monoclinic
Space group	$P2_1/c$	$P2_1$
a/Å	7.0070(4)	10.1199(6)
b/Å	12.7983(7)	16.2239(10)
c/Å	18.8563(11)	11.8583(8)
α/°	90	90
β/°	90.618(2)	114.402(2)
γ/°	90	90
Volume/Å^3	1690.89(17)	1773.02(19)
Z	4	2
ρ_{calc}g/cm^3	1.695	1.732
μ/mm^{-1}	1.277	1.026
F(000)	880.0	954.0
Crystal size/mm^3	0.362 × 0.078 × 0.052	0.273 × 0.175 × 0.067
Radiation	Mo Kα (λ = 0.71073)	Mo Kα (λ = 0.71073)
2Θ range for data collection/°	6.36 to 60.24	6.28 to 66.48
Index ranges	$-9 \le h \le 9$, $-18 \le k \le 18$, $-26 \le l \le 26$	$-15 \le h \le 15$, $-24 \le k \le 24$, $-18 \le l \le 18$
Reflections collected	28307	33419
Independent reflections	4963 [R_{int} = 0.0829, R_{sigma} = 0.0804]	13522 [R_{int} = 0.0435, R_{sigma} = 0.0791]
Data/restraints/parameters	4963/0/208	13522/1/490
Goodness-of-fit on F^2	1.063	0.991
Final R indexes [I>=2σ (I)]	R_1 = 0.0520, wR_2 = 0.0894	R_1 = 0.0499, wR_2 = 0.0970
Final R indexes [all data]	R_1 = 0.1045, wR_2 = 0.1039	R_1 = 0.0829, wR_2 = 0.1087
Largest diff. peak/hole / e Å^{-3}	1.25/-0.55	1.31/-0.49

Table S4. Selected Bond distances (Å) for $[Mn(pyclen)Cl_2][ClO_4]$.

Bond Angles (°)	$[Mn(pyclen)Cl_2][ClO_4]$
N(1)-Mn(1)-N(2)	80.18(9)
N(1)-Mn(1)-N(3)	149.22(9)
N(1)-Mn(1)-N(4)	77.56(9)
N(2)-Mn(1)-N(3)	80.81(9)
N(2)-Mn(1)-N(4)	87.33(10)
N(3)-Mn(1)-N(4)	77.58(1)
N(1)-Mn(1)-Cl(1)	97.22(7)
N(1)-Mn(1)-Cl(2)	104.44(7)
N(2)-Mn(1)-Cl(1)	174.76(8)
N(2)-Mn(1)-Cl(2)	88.60(7)
N(3)-Mn(1)-Cl(1)	99.62(7)
N(3)-Mn(1)-Cl(2)	99.06(7)
N(4)-Mn(1)-Cl(1)	87.67(7)
N(4)-Mn(1)-Cl(2)	175.09(7)
Cl(1)-Mn(1)-Cl(2)	96.48(3)

Table S5. Selected Bond distances (Å) for $[Mn_2(pyclen)_2(\mu\text{-}O)_2][ClO_4]_3$.

Bond Distances (Å)	$[Mn_2(pyclen)_2(\mu\text{-}O)_2][ClO_4]_3$
Mn(1)-N(1)	2.086(3)
Mn(1)-N(2)	2.091(3)
Mn(1)-N(3)	2.090(3)
Mn(1)-N(4)	1.991(3)
Mn(1)-O(1)	1.809(2)
Mn(1)-O(2)	1.800(2)
Mn(1)-Mn(2)	2.712(7)
Mn(2)-O(1)	1.861(2)
Mn(2)-O(2)	1.849(2)
Mn(2)-N(5)	2.246(3)
Mn(2)-N(6)	2.110(3)
Mn(2)-N(7)	2.266(3)
Mn(2)-N(8)	2.058(3)

Table S6. Selected Bond Angles (°) for $[Mn(pyclen)Cl_2][ClO_4]$.

Bond Angles (°)	$[Mn(pyclen)Cl_2][ClO_4]$
N(1)-Mn(1)-N(2)	80.18(9)
N(1)-Mn(1)-N(3)	149.22(9)
N(1)-Mn(1)-N(4)	77.56(9)
N(2)-Mn(1)-N(3)	80.81(9)
N(2)-Mn(1)-N(4)	87.33(10)
N(3)-Mn(1)-N(4)	77.58(1)
Mn(1)-O(1)-Mn(2)	-
Mn(1)-O(2)-Mn(2)	-
O(1)-Mn(1)-O(2)	-
O(1)-Mn(2)-O(2)	-

Table S7. Selected Bond Angles (°) for $[Mn_2(pyclen)_2(\mu\text{-}O)_2][ClO_4]_3$.

Bond Angles (°)	$[Mn_2(pyclen)_2(\mu\text{-}O)_2][ClO_4]_3$	$[Mn(pyclen)Cl_2][ClO_4]$
N(1)-Mn(1)-N(2)	81.90(13)	80.18(9)
N(1)-Mn(1)-N(3)	153.83(11)	149.22(9)
N(1)-Mn(1)-N(4)	80.16(14)	77.56(9)
N(2)-Mn(1)-N(3)	81.49(13)	80.81(9)
N(2)-Mn(1)-N(4)	89.60(11)	87.33(10)
N(3)-Mn(1)-N(4)	79.65(14)	77.58(1)
Mn(1)-O(1)-Mn(2)	95.26(11)	-
Mn(1)-O(2)-Mn(2)	95.97(11)	-
O(1)-Mn(1)-O(2)	85.81(11)	-
O(1)-Mn(2)-O(2)	82.96(10)	-
N(1)-Mn(1)-O(1)	100.68(14)	-
N(1)-Mn(1)-O(2)	100.36(14)	-
N(2)-Mn(1)-O(1)	176.48(12)	-
N(2)-Mn(1)-O(2)	91.37(11)	-
N(3)-Mn(1)-O(1)	96.90(14)	-
N(3)-Mn(1)-O(2)	100.11(14)	-
N(4)-Mn(1)-O(1)	93.20(11)	-
N(4)-Mn(1)-O(2)	178.96(12)	-
N(1)-Mn(1)-Cl(1)	-	97.22(7)
N(1)-Mn(1)-Cl(2)	-	104.44(7)
N(2)-Mn(1)-Cl(1)	-	174.76(8)
N(2)-Mn(1)-Cl(2)	-	88.60(7)
N(3)-Mn(1)-Cl(1)	-	99.62(7)
N(3)-Mn(1)-Cl(2)	-	99.06(7)
N(4)-Mn(1)-Cl(1)	-	87.67(7)
N(4)-Mn(1)-Cl(2)	-	175.09(7)
Cl(1)-Mn(1)-Cl(2)	-	96.48(3)
N(5)-Mn(2)-N(6)	80.29(14)	-
N(5)-Mn(2)-N(7)	148.37(11)	-

Mn(5)-Mn(2)-N(8)	77.98(13)	-
N(5)-Mn(2)-O(1)	102.96(13)	-
N(5)-Mn(2)-O(2)	100.86(13)	-
N(6)-Mn(2)-N(7)	79.57(14)	-
N(6)-Mn(2)-N(8)	88.39(11)	-
N(6)-Mn(2)-O(1)	95.38(11)	-
N(6)-Mn(2)-O(2)	178.14(12)	-
N(7)-Mn(2)-N(8)	77.32(13)	-
N(7)-Mn(2)-O(1)	102.99(13)	-
N(7)-Mn(2)-O(2)	99.97(13)	-
N(8)-Mn(2)-O(1)	176.21(11)	-
N(8)-Mn(2)-O(2)	93.27(11)	-

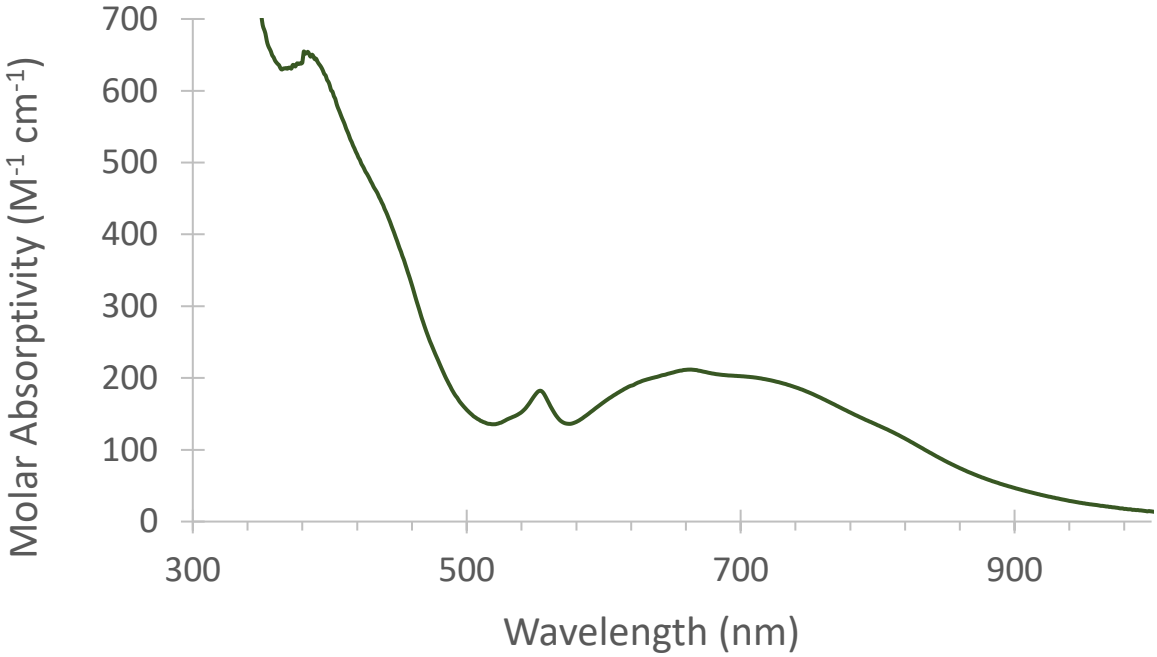

Figure S1. Electronic spectrum of $[Mn_2(pyclen)_2(\mu\text{-}O)_2][ClO_4]_3$ in H_2O.

Analysis of $[Mn_2(pyclen)_2(\mu\text{-}O)_2]^{3+}$ EPR spectra.

The valence-localized Mn^{III} and Mn^{IV} sites within the $[Mn_2(pyclen)_2(\mu\text{-}O)_2]^{3+}$ complex are inequivalent, therefore the observed (*system*) g_s- and A_s-values obtained from the experimental spectrum are comprised of intrinsic values from each ion weighted by their projections onto the total spin-system [equation (**S3**) and (**S4**), respectively]. From equations (**S5**) and (**S6**), the spin-projection coefficients [c_1 = 2 and c_2 = -1] within the coupled (S = 1/2) $Mn^{III}Mn^{IV}$-cluster can be calculated for intrinsic Mn^{III} (S_1 = 2) and Mn^{IV} (S_2 = 3/2) sites, respectively.[2]

$$\textbf{(3)} \qquad g_s = c_1 g_1 + c_2 g_2 = 2g_1 - g_2$$

$$\textbf{(4)}\ A_s = c_1 A_1 + c_2 A_2 = 2A_1 - A_2$$

$$\textbf{(5)}\ c_1 = \frac{S_1(S_1+1) - S_2(S_2+1) + S(S+1)}{S(S+1)}\ ;\ \textbf{(6)}\ c_2 = \frac{S_2(S_2+1) - S_1(S_1+1) + S(S+1)}{S(S+1)}$$

Table S8 summarizes the system g-values and intrinsic Mn^{III} and Mn^{IV} A-values obtained. As indicated by equation (**S3**), the system g- and A-values for $[Mn_2(pyclen)_2(\mu\text{-}O)_2]^{3+}$ are dominated by the Mn^{III}-site as its spin-projection is 2-fold greater than that of Mn^{IV}-site. Reported g-values for Mn^{III} (d^4) and Mn^{IV} (d^3) ions exhibit small, but non-zero, deviations from the free electron g-value (g_e).[3,4,5,6] At X-band, this g-anisotropy can be difficult to accurately resolve and thus deconvolution of system g-values for $[Mn_2(pyclen)_2(\mu\text{-}O)_2]^{3+}$ into intrinsic contributions from Mn^{III} and Mn^{IV} ions is unreliable.

Table S8. *Selected EPR spectroscopic parameters for $[Mn_2(pyclen)_2(\mu\text{-}O)_2][ClO_4]_3$ and $[Mn_2(cyclen)_2(\mu\text{-}O)_2][ClO_4]_3$ obtained from simulation compared to literature examples.*

Ligand	system [g_1, g_2, g_3]	intrinsic Mn^{III} $\lvert[A_x, A_y, A_z]\rvert$ (MHz)[a]	intrinsic Mn^{IV} $\lvert[A_x, A_y, A_z]\rvert$ (MHz)	Mn^{III} (A_{iso})	Mn^{IV} (A_{iso})	A_1/A_2
pyclen	2.024, 2.010, 2.017	467, 453, 418	239, 207, 198	446 MHz	215 MHz	2.08
cyclen	2.023, 2.007, 2.016	487, 450, 416	237, 205, 194	451 MHz	212 MHz	2.13
Mn-CAT^{Lp}	2.008, 2.008, 1.990	312, 312, 426	251, 251, 228	350 MHz	243 MHz	1.44
Mn-CAT^{Tt}	2.014, 2.014, 2.000	315, 425, 410	252, 224, 235	383 MHz	237 MHz	1.62
Mn-CAT^{Tt}	2.006, 2.004, 2.004	444, 405, 405	216, 210, 210	418 MHz	212 MHz	1.97
Mn_2-bpy	2.030, 3.030, 2.030	468, 468, 469	222, 222, 222	468 MHz	222 MHz	2.11
$Mn_2(O)(Oac)_2$	2.002, 2.001, 1.985	326, 474, 436	235, 213, 226	412 MHz	225 MHz	1.83

[a] Experimental measurements performed here only report the magnitude of hyperfine splitting. However, previous studies on various Mn-complexes have found that the intrinsic hyperfine values for manganese are negative.[3, 7-9] Data reported for manganese catalase (Mn-CAT) isolated from *Lactobacillus plantarum*[10,11] and *Thermus thermophilus.*[12,13] EPR spectroscopic parameters for $Mn^{III}Mn^{IV}$-complexes for Mn_2-bpy and $Mn_2(O)(Oac)_2$ reported elsewhere.[11]

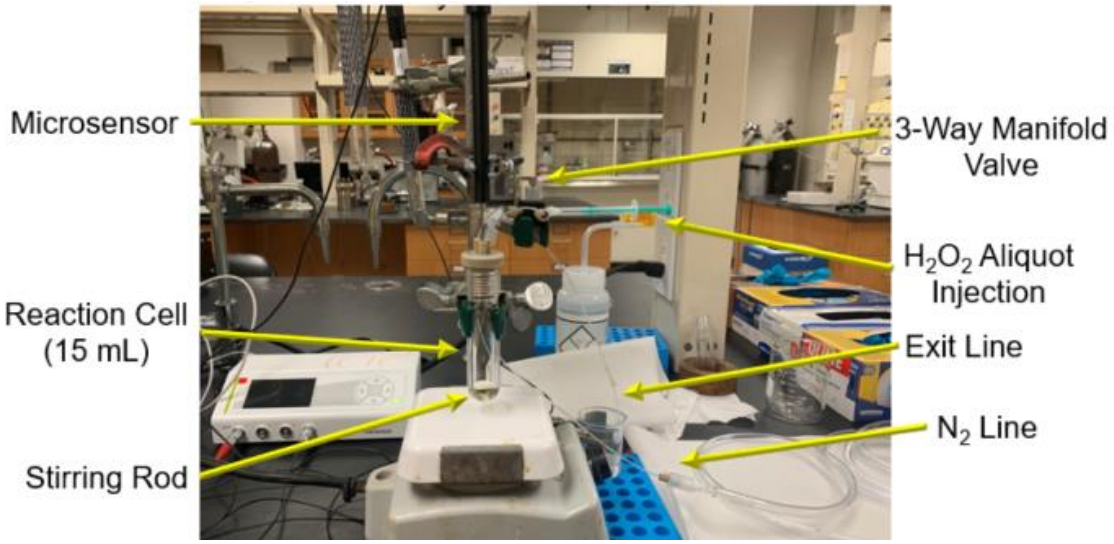

Figure S2. O_2 measurement setup using an O_2 microsensor (Unisense) for quantifying O_2 produced by H_2O_2 disproportionation.

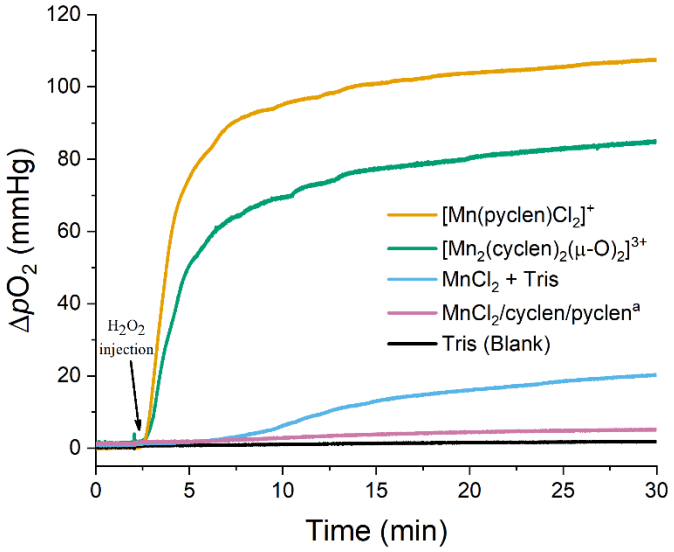

Figure S3. Dioxygen formation from hydrogen peroxide disproportionation catalyzed by manganese complexes of cyclen (green) and pyclen (orange) at pH 8 and control reactions with $MnCl_2$ + Tris buffer (blue), $MnCl_2$ without any ligand (pink) ([a]note that an overlapping result was obtained when $MnCl_2$ was replaced with either pyclen or cyclen in this control experiment), and for buffer alone (black). Initial conditions: $[Mn^{2+}]$ = 1.5 mM, [ligand] = 1.54 mM, $[H_2O_2]$ = 150 mM, [buffer] = 50 mM.

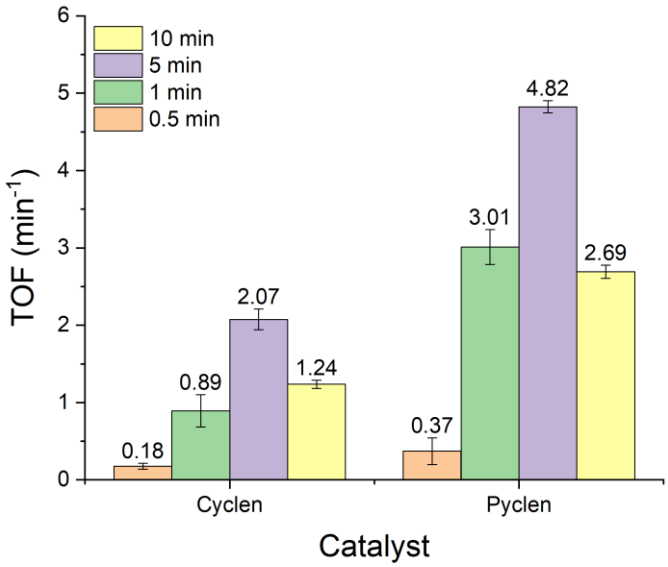

Figure S4. TOF values calculated from the start of the H_2O_2 disproportionation reaction for the Mn complexes with cyclen and pyclen at pH 8. Initial conditions: [Mn^{2+}] = 1.5 mM, [ligand] = 1.54 mM, [H_2O_2] = 150 mM, [buffer] = 50 mM.

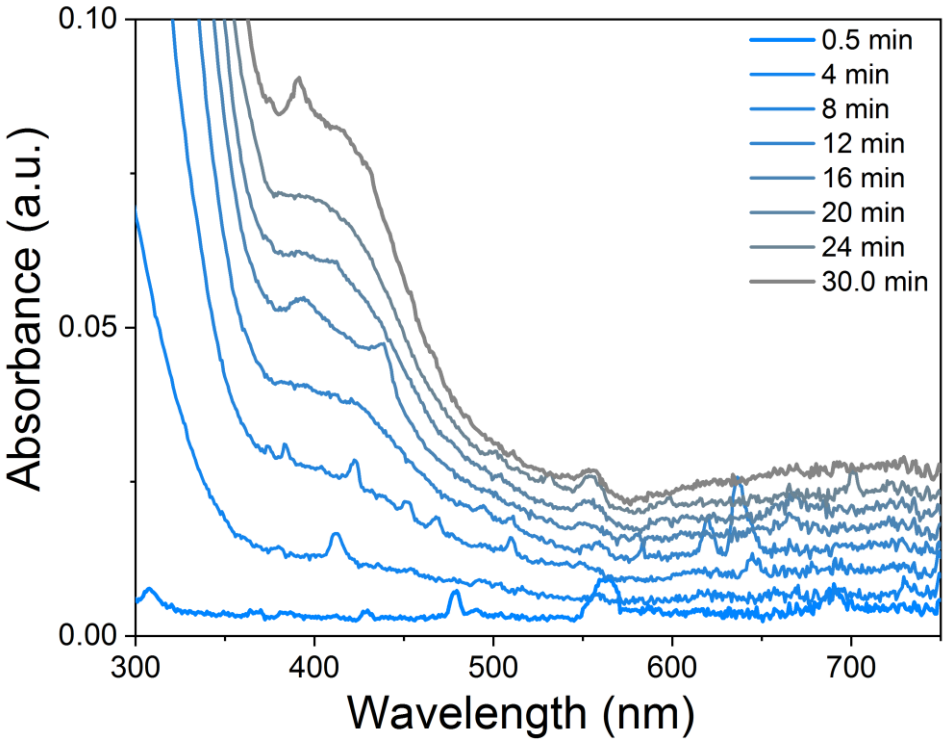

Figure S5. Absorbance spectra of cyclen-Mn in pH 8 solution measured starting from 0.5 min after the $MnCl_2$ was added to solution (dark blue) to 30 min following the addition of the Mn^{II} salt. The absorbance of solution containing only cyclen is omitted because the apparent absorption was above 0.1 absorbance units, likely do to scattering from aggregates present in solution. Initial conditions: 2 mM $MnCl_2$, 2.04 mM cyclen, 50 mM Tris buffer.

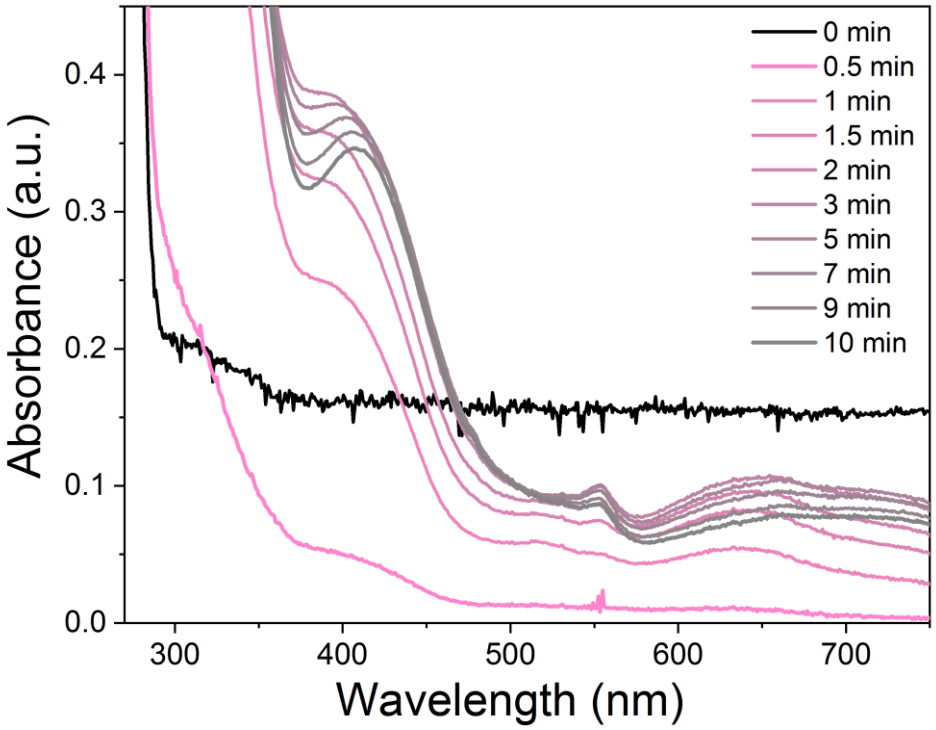

Figure S6. Absorbance spectra of pyclen-Mn in pH 8 solution measured starting from only pyclen present in solution (black) to 10 min after the $MnCl_2$ was added to solution (dark grey). Initial conditions: 2 mM $MnCl_2$, 2.04 mM pyclen, 50 mM Tris buffer). Spectra of the ligand in the absence of Mn(II) salt showed elevated absorbance across the visible range, attributed to particulate scattering, compared to the baseline taken of neat buffered solution.

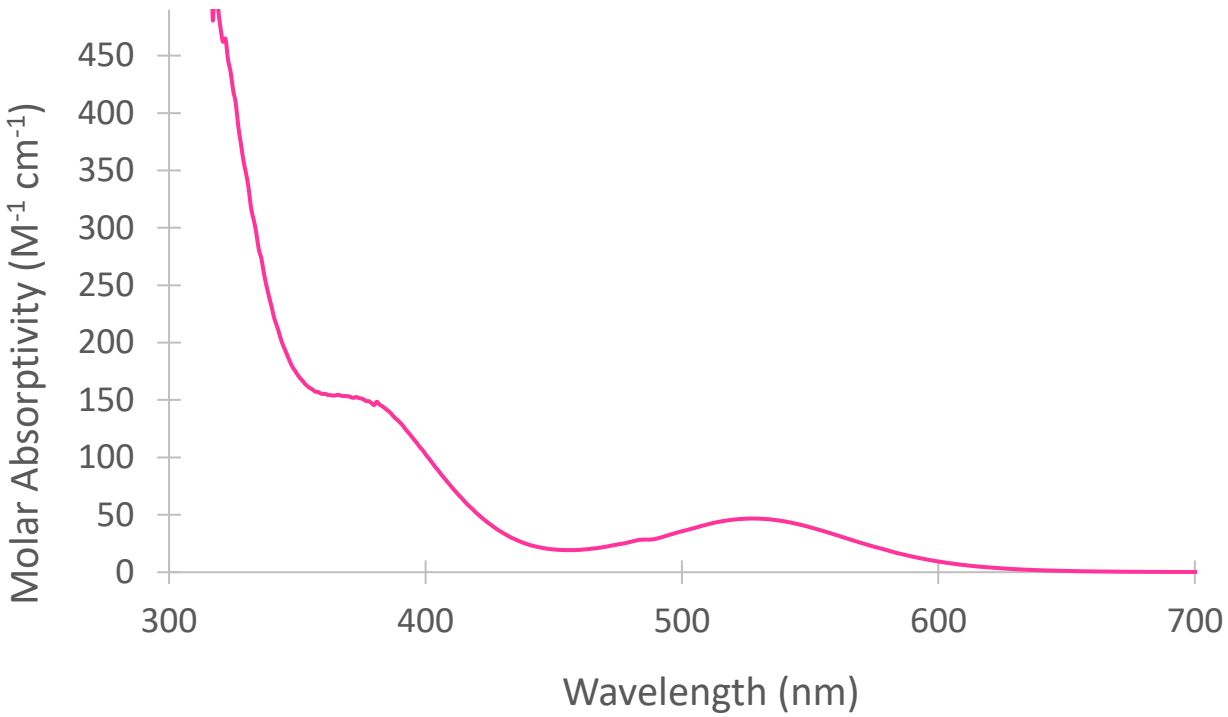

Figure S7. Electronic spectrum of $[Mn(pyclen)Cl_2][ClO_4]$ in CH_3CN.

References

1. Green, K. N.; Pota, K.; Tircsó, G.; Gogolák, R. A.; Kinsinger, O.; Davda, C.; Blain, K.; Brewer, S. M.; Gonzalez, P.; Johnston, H. M.; Akkaraju, G., Dialing in on pharmacological features for a therapeutic antioxidant small molecule. *Dalton Transactions* **2019,** *48*, 12430-12439.
2. Bencini, A.; Gatteschi, D., *Electron Paramagnetic Resonance of Exchange Coupled Systems*. Springer: Heidelberg, 1990.
3. Campbell, K. A.; Yikilmaz, E.; Grant, C. V.; Gregor, W.; Miller, A.-F.; Britt, R. D., Parallel Polarization EPR Characterization of the Mn(III) Center of Oxidized Manganese Superoxide Dismutase. *Journal of the American Chemical Society* **1999,** *121* (19), 4714-4715.
4. Krzystek, J.; Yeagle, G. J.; Park, J.-H.; Britt, R. D.; Meisel, M. W.; Brunel, L.-C.; Telser, J., High-Frequency and -Field EPR Spectroscopy of Tris(2,4-pentanedionato)manganese(III): Investigation of Solid-State versus Solution Jahn−Teller Effects. *Inorganic Chemistry* **2003,** *42* (15), 4610-4618.
5. Gupta, R.; Taguchi, T.; Lassalle-Kaiser, B.; Bominaar, E. L.; Yano, J.; Hendrich, M. P.; Borovik, A. S., High-spin Mn–oxo complexes and their relevance to the oxygen-evolving complex within photosystem II. *Proceedings of the National Academy of Sciences* **2015,** *112* (17), 5319.
6. Leto, D. F.; Massie, A. A.; Colmer, H. E.; Jackson, T. A., X-Band Electron Paramagnetic Resonance Comparison of Mononuclear Mn(IV)-oxo and Mn(IV)-hydroxo Complexes and Quantum Chemical Investigation of MnIV Zero-Field Splitting. *Inorganic Chemistry* **2016,** *55* (7), 3272-3282.
7. Abragam, A.; Bleaney, B., *Electron Paramagnetic Resonance of Transition Ions (International Series of Monographs on Physics)*. 1970; p 912 pp.
8. Campbell, K. A.; Yikilmaz, E.; Grant, C. V.; Gregor, W.; Miller, A.-F.; Britt, R. D., Parallel Polarization EPR Characterization of the Mn(III) Center of Oxidized Manganese Superoxide Dismutase. *J Am Chem Soc.* **1999,** *121* (19), 4714-4715.

9. Zheng, M.; Khangulov, S. V.; Dismukes, G. C.; Barynin, V. V., Electronic structure of dimanganese(II,III) and dimanganese(III,IV) complexes and dimanganese catalase enzyme: a general EPR spectral simulation approach. *Inorg Chem.* **1994,** *33* (2), 382-387.
10. Pierce, B. S.; Hendrich, M. P., Local and Global Effects of Metal Binding within the Small Subunit of Ribonucleotide Reductase. *J Am Chem Soc.* **2005,** *127* (10), 3613-3623.